GROWTH OF AISЬ ON INSULATING SUBSTRATES BY METAL ORGANICS CHEMICAL VAPOUR DEPOSITION

Mathieu LEROUX, Annie TROMSON-CARLI, Pierre GIBART and Christian VÉRIÉ

Laboratoire de Physique des Solides, Laboratoire de Magnétisme, CNRS, F-92190 Meudon-Bellevue, France

and

Claude BERNARD and Marie Claude SCHOULER

Centre d'Information de Thermodynamique Chimique Minérale ENSEEG, BP 44, F-38401 Saint Martin d'Hères, France

Received 21 July 1979; manuscript received in final form 5 October 1979

Aluminium antimonide thin films were grown on different insulating substrates, i.e. silica, CaF₂, BaF₂, Al₂O₃, GaAs, by metal organics chemical vapour deposition (MO-CVD). Epitaxial AlSb thin films were successfully grown on CaF₂ and GaAs. In the process, the metal alkyls trimethylaluminium (TMA) and trimethylantimony (TMSb) are the sources of Al and Sb, respectively. The thermodynamic study of the system Al-Sb-C-H shows that AlSb could be deposited for given values of the partial pressures of Al, Sb and C in the vapour phase. Other condensed phases could appear, Al₄C₃, Sb.

1. Introduction

MO-CVD has been shown in the last decade to be a reliable alternative to the technique using halides [1]. Single crystal thin films of GaAs were grown, with electrical quality comparable to those obtained from halides.

In the MO-CVD process, III—V compounds are usually formed by reaction of a Group III element alkyl in the presence of a Group V element hydride. However, in the case of antimonide, SbH₃ is instable at room temperature and is therefore not available. In the present work TMSb was used as Sb source. In the case of aluminium compounds, usual growth methods like vapour phase epitaxy (VPE) or liquid phase epitaxy (LPE) are difficult to achieve because gaseous aluminium chloride etches the quartz tubes and molten aluminium etches all common crucibles. In VPE of Al compounds an alumina reactor ought to be used. In both processes, special precautions are to be taken towards preventing any traces of oxygen.

In the past several techniques have been used for growing AlSb. Single crystal needles were grown from the vapour using chlorine [2] as transport agent.

Considerable etching of the quartz tube occurs and this method is not reliable to grow pure large single crystals of AlSb.

Crystal growth of AlSb from the melt was not successfull: molten aluminium and antimony have large differences in density so that a good homogeneity of the ingot cannot be reached [3] and an intergranular Al-rich impurity phase is formed. AlSb was even tentatively grown from the melt in the Apollo—Soyuz test project (ASTP) [4]; the quality of the ingots obtained was much better than on earth but the result was not a real AlSb single crystal. The intergranular phase was almost eliminated.

AlSb thin films were grown by vacuum evaporation by several authors [5,6]. Films were either polycrystalline or inhomogeneous, and atmospheric deterioration occurs after some time. Homogeneous stoichiometric AlSb films were deposited by Johnson; the high resistivity of these films did not allow any transport measurement [7]. AlSb thin films, with semiconducting properties close to the bulk samples were obtained by coevaporation [8].

Strong photovoltaic response was obtained with AlSb films on Ta contacts prepared by evaporation [9]. Polycrystalline AlSb was obtained by dc sputtering in high purity argon atmosphere [10].

To our knowledge, no VPE study of AlSb has been reported so far. This paper deals with the growth of AlSb using a MO-CVD method. After a brief survey of the characteristics of this compound as a potential photovoltaic material [11,12], the thermochemistry aspect is discussed in section 3. The results obtained under various conditions are reported in section 4, emphasizing the precise control of the growth parameters needed for high quality epitaxy.

2. AlSb as a candidate material for photovoltaic solar energy conversion

After the pioneer work of Loferski [13] and Rappaport [14] devoted to the electronic structure and materials aspects of the optimization of high efficiency solar cells, a number of II—VI and III—V semiconductors have been proposed. AlSb, which has already been mentioned [14], offers interesting properties. However the great difficulties to grow AlSb single crystal or thin films have limited the investigations of AlSb solar cells. This paragraph deals with a survey of the main properties of this compound having some importance in the framework of solar photovoltaics, i.e. ionicity, availability of photovoltaic material and band structure features.

2.1. Ionicity

Comparing the results obtained so far with various materials, it appears that Si, GaAs, and InP, i.e. covalent or quasi-covalent materials, exhibit the highest efficiency. This property indicates that among the material selection criteria for high efficiency solar cells, ionicity is a basic parameter which was underestimated. As a result the III-V compounds with

their weak ionicity have consequently few native defects or impurity--defect complexes and practically no self-compensation effect. The III -V semiconductors are the most promising candidate for achieving high efficiency solar cells. The III-V compound AlSb is expected to share these general properties, provided a suitable crystallization technique could be set up, avoiding segregation effects induced by gravity effects at the liquid-solid interface [4]. Undoped AlSb was always found to be p-type with $p \simeq 10^{17} \text{ cm}^{-3}$. This native defect, probably due to high Sb vacancy concentration, may be related to these segregation effects. A method like MO-CVD could avoid these difficulties. Furthermore, as shown in the deposition of GaAs by MO-CVD, the control of the ratio Sb/Al in the gas could allow a control of the stoichiometry. As a result, this Sb/Al ratio control might have a strong influence on the p-type native defect concentration.

2.2. Availability of photovoltaic materials

Among the nearly ideal band-gap compounds for solar energy, i.e. InP, GaAs, CdTe and AlSb [4], the latter has no problem of constituent element abundance, even in the case of large scale photovoltaic central station power plants working without concentration (see table 1 restricted to the III—V family).

Note the necessity of high concentration ($C \ge 200$) for materials like GaAs and InP and for any alloy using Ga or In. This implies the achievement of very high efficiency solar cells with such elements since this parameter is crucial for high concentration converters.

2.3. Band structure features

Solar cells are usually parametrized through three main quantities: the open circuit voltage $V_{\rm OC}$, the short circuit current $I_{\rm SC}$ and the "fill factor" [13]. Usually the optimized efficiency of a solar cell is

Table 1
Abundance (in metric tons) of elements

Elements	Al	Ga	In	As	Sb
World reserves	1.17 × 10 ⁹	1.12 × 10 ⁵	1.4 × 10 ³	3.7 × 10 ⁶	7.7 × 10 ⁶

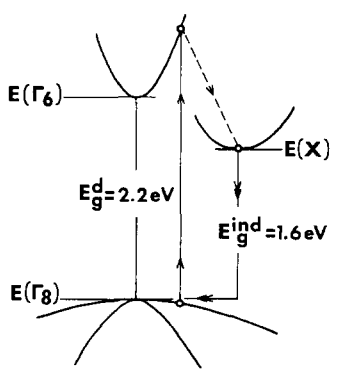


Fig. 1. Band structure scheme of AlSb. The arrows illustrate optical absorption, thermalisation and recombination processes.

mainly the result of a compromise between the achievement of the highest open circuit voltage factor $F(V_{\rm OC}) = eV_{\rm OC}/E_{\rm g}$ ($E_{\rm g}$ is the gap of the semiconductor) and the longest lifetime of minority carriers related to a diffusion length $L_{\rm D}$ compatible with the optical absorption length. In a p-n homo-junction device this is achieved at a limited doping level of the n- and p-type parts of the cell.

It has been proposed to use an indirect gap material having a band structure close to the direct—indirect gap transition, but with $E_{\rm g}^{\rm dir} \gtrsim E_{\rm g}^{\rm ind}$ and of about 1.4 eV [14]. Such a situation (fig. 1) allows to combine strong optical absorption (mainly due to transitions across the direct gap) and long intrinsic lifetime of the minority carriers (due to the thermalisation in the indirect gap configuration). Therefore the above limited doping level of the p—n function may be substantially increased, since the low doping material would have a longer lifetime. Recent photoluminescence studies of GaAs under high pressure have been interpreted, in the indirect gap configuration, with a lifetime higher than value determined in the one bar case 17.

An examination of III–V ternary alloys with appropriate Γ –L crossovers in the conduction band has stressed the importance of AlSb-based materials as good candidates [16,18]. In the framework of the above considerations (section 2.2), AlSb with $E_{\rm g}^{\rm ind}=1.6~{\rm eV}$ and $E_{\rm g}^{\rm dir}=2.2~{\rm eV}$ is attractive since it allows to avoid the use of rather rare elements such as In or Ga. Restricting the thickness of AlSb to a few microns which corresponds to an optical cutoff at about

2.0 eV, taking the GaAs solar cell parameters, i.e. a quantum efficiency of 0.9, a fill factor of 0.80 and $F(V_{\rm OC}) = 0.77$, the conversion efficiency is about 12% for AM1. A detailed discussion of the use of indirect band gap III—V semiconductors for photovoltaic conversion can be found in ref. [16].

3. Thermochemistry

The use of MO-CVD of AlSb from TMA and TMSb in $\rm H_2$ atmosphere raises the problem of the $\rm Al_4C_3$ phase formation. A thermodynamic analysis of the system Al-Sb-C-H allows to determine the different condensed phases in equilibrium with the gases. This is a reliable starting point for the deposition of AlSb.

The rate limiting process in MO-CVD could be either mass transfer (diffusion, convection turbulences) or surface reaction. Different processes have been discussed in detail in recent papers [18]. In the present study no systematic study of the speed of deposition was carried out as a function of different parameters.

A proposed mechanism for the growth of GaAs from organometallics is the formation of complexes such as $Ga(CH_3)_3$ —AsH₃ with subsequent polymerisation and desorption of CH₄. Such a mechanism cannot be considered in the case of the growth of AlSb from TMA and TMSb.

The complex Al(CH₃)₃—Sb(CH₃)₃ is weakly bound and Sb(CH₃)₃ starts to decompose at a low temperature, beginning to form elementary antimony well above the substrate (this a cause of incertitude in the knowledge of the actual Sb pressures in the reactor). The reaction responsible for the crystal growth of AlSb is then

$$Al(CH_3)_3 + \frac{1}{4}Sb_4 + \frac{3}{2}H_2 \rightarrow \langle AlSb \rangle + 3CH_4$$
. (1)

This reaction is competitive with the well known pyrolisis of the TMA [18]:

$$4 \operatorname{Al}(\operatorname{CH}_3)_3 \to \langle \operatorname{Al}_4 \operatorname{C}_3 \rangle + 9 \operatorname{CH}_4 . \tag{2}$$

The dimerisation of the TMA in the gas phase may also be relevant by preventing the formation of a III-V complex such as $(CH_3)_3Al-Sb(CH_3)_3$ and by enhancing the aluminium carbide formation.

In order to estimate the relative strength of reac-

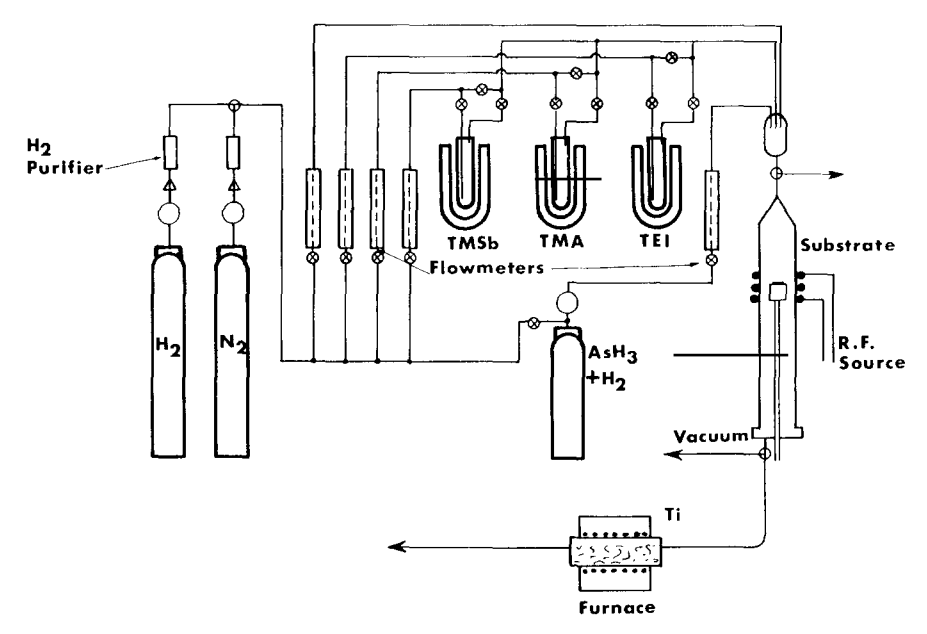


Fig. 2. Schematic equipment for MO-CVD of AlSb and InSb.

tions (1) and (2), thermodynamic calculations have been performed on the Al-Sb-C-H equilibrium system by minimisation of the system's free energy function, using the computation procedure described in ref. [21]. Considering, in accordance with the experiments, that the pyrolysis of the trimethylaluminium and the trimethylantimony are complete, the chemi-

cal species considered are: Sb, Sb₂, Sb₄, H₂, Al, CH₄ and C_2H_2 in the gas phase, and AlSb, Al, Sb, Al₄C₃ and C in the condensed phase.

No mixing is supposed to occur in the condensed phase, so that the activity of each condensed species is 1. Thermochemical data were taken from ref. [22] for AlSb, from ref. [23] for Al₄C₃, from ref. [24] for CH₄ and C_2H_2 and from ref. [25] for the other species.

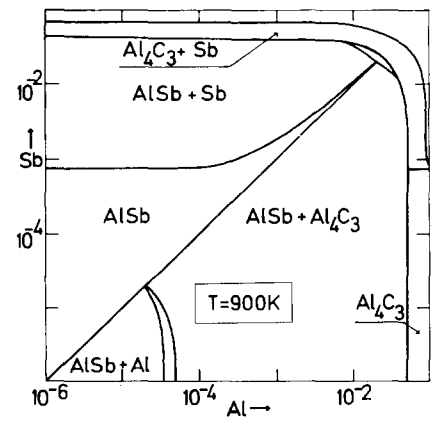


Fig. 3. Phase diagram of the Al-Sb-C-H system. The x and y axes give the molar fractions of Al and Sb, respectively (or the partial pressures of TMA and TMSb entering the reactor). T = 900 K.

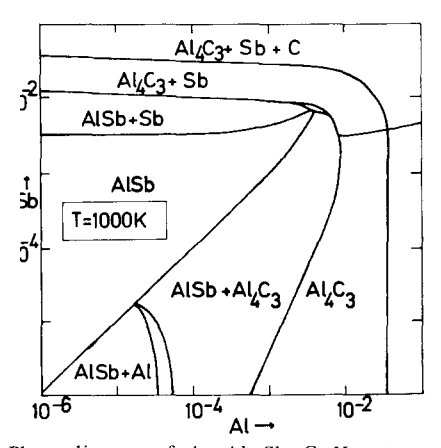


Fig. 4. Phase diagram of the Al-Sb-C-H system of fig. 3. T = 1000 K.

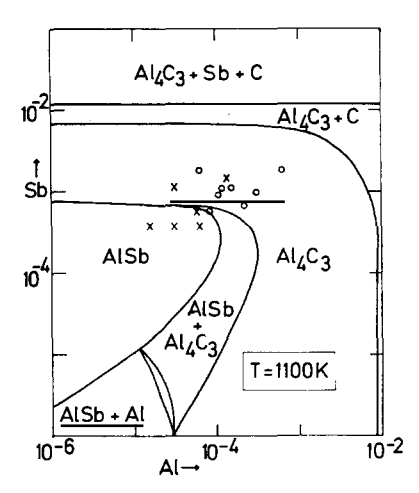


Fig. 5. Phase diagram of the Al-Sb-C-H system of fig. 3. T = 1100 K. (×) and (\circ) are experimental results around 1100 K: (×) AlSb deposit; (\circ) AlSb + Al₄C₃ deposit.

Figs. 3, 4 and 5 show the Al-Sb-C-H phase diagrams at 900, 1000 and 1100 K respectively, as a function of the Al and Sb mole fractions in the inlet gas phase, which is a mixture of Al(CH₃)₃, Sb(CH₃)₃ and H₂ (i.e. the total composition of the inlet gas phase is determined by the Al and Sb mole fractions). Figs. 3 and 4 show that at temperatures ranging from 900 to 1000 K, the domain of AlSb formation has the rough shape of a triangle limited by the stoichiometry line (Sb = Al) and the Sb deposition line $(Sb = {}^{1}P_{0}(Sb_{4}), \text{ where } P_{0}(Sb_{4}) \text{ is the equilibrium } Sb_{4}$ vapour pressure of elemental antimony). This means that AlSb deposition occurs under Sb supersaturation, which is limited by the low equilibrium vapour pressure of antimony, Po(Sb₄). The AlSb domain is then limited to a small area of the diagram which increases with temperature, together with $P_0(Sb_4)$.

At higher temperature, however, a further limitation appears due to strong aluminium carbide formation, even at very low Al concentrations (see fig. 5). Interpolating between these two limitations leads to considering that the AlSb deposition domain has the largest area at a temperature of approximately 1070 K, what has directly been observed experimentally.

On fig. 5 are shown some experimental points, showing a good qualitative agreement with theory. The reasons of the discrepancy may be attributed to an overestimation of the Sb content of the gas phase

and to the fact that Sb/Al ratios larger than 1 are needed to grow AlSb, presumably due to kinetic effects that our equilibrium model cannot account for (see section 4).

4. Experimental results

4.1. Experimental conditions

MO-CVD of AlSb was obtained from the reaction between TMA and TMSb on a hot substrate at high temperature (1000–1100 K). The system used in these experiments is schematically drawn on fig. 2.

A vertical reactor was used with typical dimensions: diameter 5 cm and heigth 50 cm. Gases are introduced in the reactor at the conical end to avoid turbulences. The graphite susceptor was heated by a radio frequency induction heating system. The temperature was monitored by a Pt/Pt—Rh thermocouple enclosed in a quartz tube inserted into the susceptor.

The metalorganics (Alfa) were supplied in stainless steel bottles fitted with bubbler tubes. The concentration of TMA and TMSb in the gas phase was determined by controlling the temperature of the bottles: TMA was kept at 25° C (12 Torr) whereas TMSb at 0° C (29 Torr) or -32° C (6 Torr). Vapours of the metalorganics were transported to the reactor by bubbling pure hydrogen through the liquids. H_2 passed over a chemical purifier.

The different hydrogen flows (saturated with TMA, TMSb and the carrier gas respectively) where premixed before entering in the reactor.

All gas lines and valves are in stainless steel. The different flows were accurately controlled by mass flowmeters. Special effort was done to avoid any leak in the tubing system. After leaving the reactor, the exhaust gases pass over chromium kept at 1100 K (free Sb reacts with chromium) and different bubblers.

In a standard run, the reactor is first evacuated, then flushed by N_2 and finally by H_2 . The insulating substrate is heated up to the deposition temperature, then the TMSb flow is admitted into the reactor, and 5 min later the TMA flow. The insulating substrate was mechanically polished with diamant abrasive ending with 0.5 μ m grade. A specific standard etching process is done for each kind of substrate.

Run	H ₂ flow (ml/min)	$p(\text{TMA}) = 2p(\text{Al}_2(\text{CH}_3)_6)$ (10 ⁻⁴ atm)	p(TMSb) (10 ⁻⁴ atm)	Sb/Al	T(K)	Result
135	4000	0.15	3.5	23	1123	AlSb
136	4000	0.15	3.5	23	1073	AlSb
154	4000	0.15	3.5	23	1023	AlSb
145	4000	0.15	3.5	23	1023	$AlSb + Al_4C_3$
141	4000	0.15	3.5	23	973	$Al_4C_3 + AlSb$

Table 2
Deposition on amorphous substrates: influence of the temperature on the nature of the deposit

4.2. Deposition on amorphous and polycrystalline substrates

No AlSb substrates are available; MO-CVD experiments were carried out either on amorphous SiO₂, or on insulating substrates with lattice parameter matching as good as possible.

The first experiments were carried out on amorphous SiO_2 or sintered Al_2O_3 to define the deposition condition of AlSb. Pertinent data of different experiments carried out in the system TMA: TMSb: H_2 are given in tables 2 and 3. Table 2 shows the influence of the deposition temperature on the nature of the deposit, the flow conditions and the partial pressures of MO are the same in all runs. Table 3 gives results for different H_2 total fluxes (in all cases <4000 ml/min) and for different Sb/Al ratios.

It can be deduced from these typical results that a qualitative agreement with the theoretical phase diagram does exits. However, the calculations were carried out assuming equilibrium, which is, of course, not the case. Furthermore, hydrogen passing through the MO is not completely saturated so that the MO

partial pressure is overestimated (this has been checked experimentally). Partial decomposition of TMSb occurs before arriving on the substrate. Partial pressures in tables 2 and 3 are overestimated. The nature of the substrate is of critical importance for the surface reactions occurring on the substrate.

After this discussion it can be concluded that a thermodynamic analysis is a useful tool to define the deposition conditions of AlSb. Formation of AlSb occurs at $T > 1000 \, \text{K}$ for Sb/Al $\lesssim 20$; for lower values of Sb/Al, Al₄C₃ is formed. These results are in good agreement with the thermodynamic conclusions.

4.3. Deposition on single crystal substrates

Several insulating substrates with unit cell parameters as close as possible as AlSb were chosen. Table 4 gives the lattice parameters of the different substrates, which were used, and the results, the conditions of growth of AlSb on these different substrates for T = 1073 K.

CaF₂. Smooth epitaxial films were grown on

Table 3
Deposition on amorphous substrates: influence of the flow conditions on the nature of the deposit

Run	H ₂ flow (ml/min)	$p(\text{TMA}) = 2p(\text{Al}_2(\text{CH}_3)_6)$ (10 ⁻⁴ atm)	p(TMSb) (10 ⁻⁴ atm)	Sb/Al	T(K)	Result
52	1100	6.13	18	3	1223	Al ₄ C ₃
50	3100	2.1	6.3	3	1123	AlSb + AlaC3
47	2100	0.31	12	38	1123	AlSb
53	1250	0.31	7.5	23	1023	AlSb
93	2100	0.32	7.6	24	953	AlSb
13	2100	1.1	9.3	9	948	AlSb + Al ₄ C ₃

Table 4						
Lattice	parameters of	possible	substrates f	or AlSb	epitaxial g	growth

Material	Substrates	a ₀ (A)	$\alpha (K^{-1})$	Results
AlSb		6.1355	4.88 × 10 ⁻⁶	No substrates available
	CaF ₂ { 111}	5.4626	10.53×10^{-6}	Epitaxial films with high degree of strains
	BaF ₂ {111}	6.2001	18.4 × 10 ⁻⁶	Decomposed by the vapour
	$Ca_3Mn_2Ge_3O_{12}$ {111}	12.320 = 2a AlSb	~9 × 10 ⁻⁶	Decomposed by the vapour
	Al ₂ O ₃ {0001}	a = 4.758 $c = 12.991$	$c \simeq 7.7 \times 10^{-6}$	Polycrystalline or textured films
	GaAs {100}	5.6419	5 × 10 ⁻⁶	Epitaxial growth

 $\langle 111 \rangle$ under the conditions reported on table 2 (sample No. 192). However, due to the large mismatch only very thin films $\leq 1 \mu m$, slowly cooled from the deposition temperature, can be grown.

Thicker films cracked during cooling, but were specular at the deposition temperature. Fig. 6 shows the surface of an AlSb film grown on (111)CaF₂ as viewed by scanning electron microscope (SEM). The

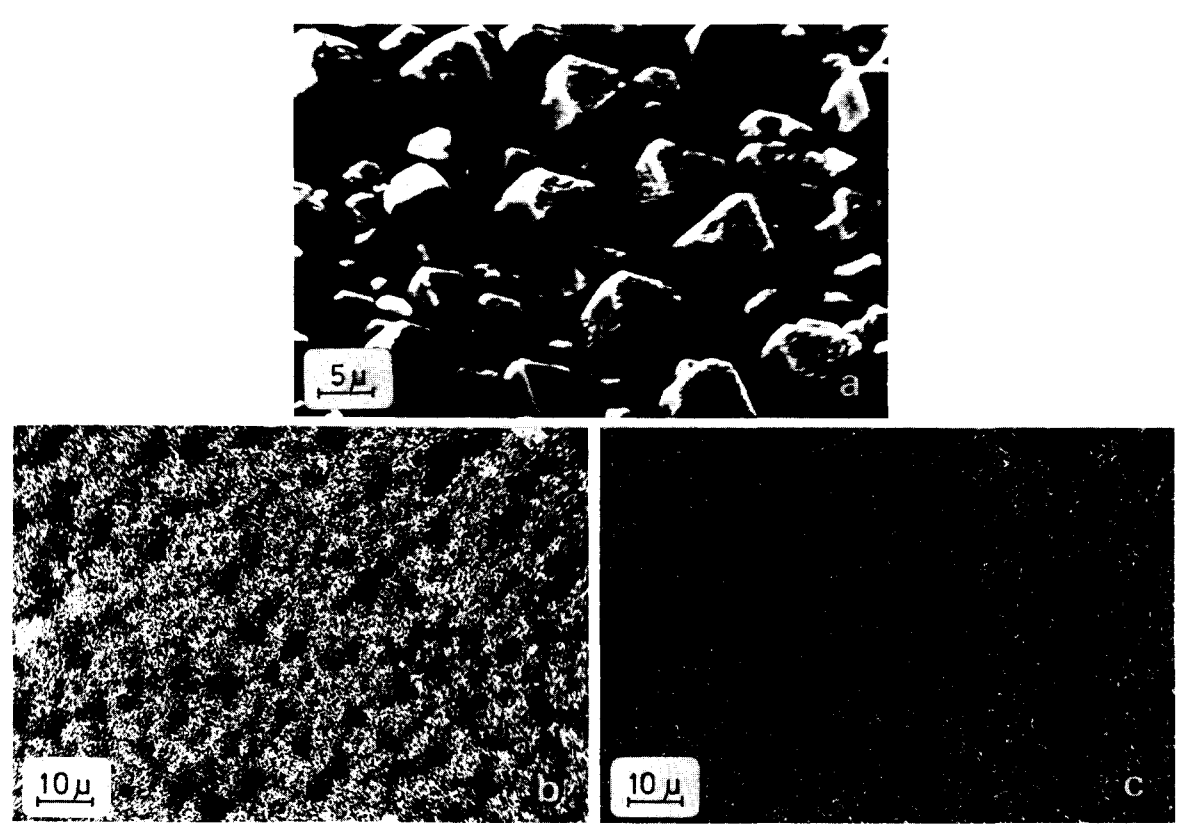


Fig. 6. SEM analysis of AlSb on (111)CaF₂ (sample No. 192): (a) surface morphology; (b) and (c) X-ray dispersive analysis $(Al(K_{\alpha}))$ and $(Al(K_{\alpha}))$ respectively).

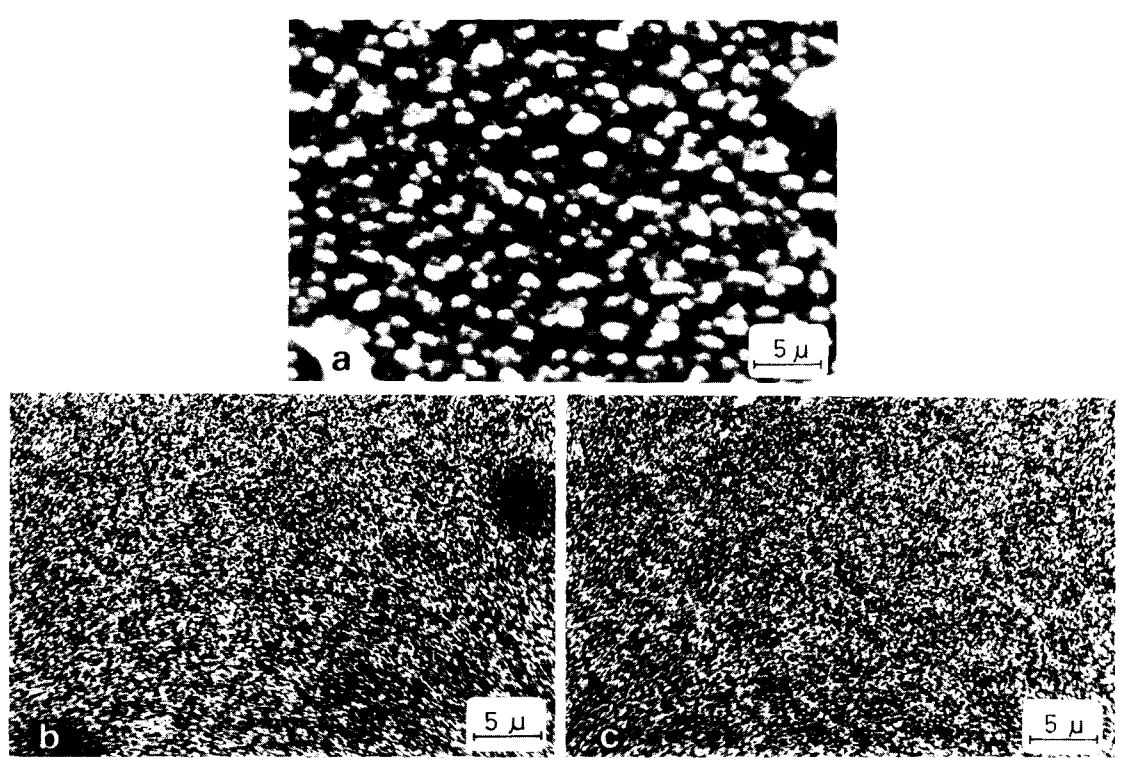


Fig. 7. SEM analysis of AlSb on CaF_2 (sample No. 62) Sb micronodules appear at the surface of the layer: (a) surface morphology; (b) and (c) X-ray dispersive analysis $(Al(K_{\alpha})$ and $Sb(L_{\alpha})$ respectively).

surface shows separated islands with $\{111\}$ facets. This is expected from the large mismatch between both the lattice parameter and the thermal expansion coefficient of the CaF_2 substrate and the AlSb film.

The X-ray analysis gives no evidence of carbon contamination (fig. 6) and shows a remarkable homogeneity of the film. Fig. 7 shows the same feature as sample No. 192, but some extra Sb was

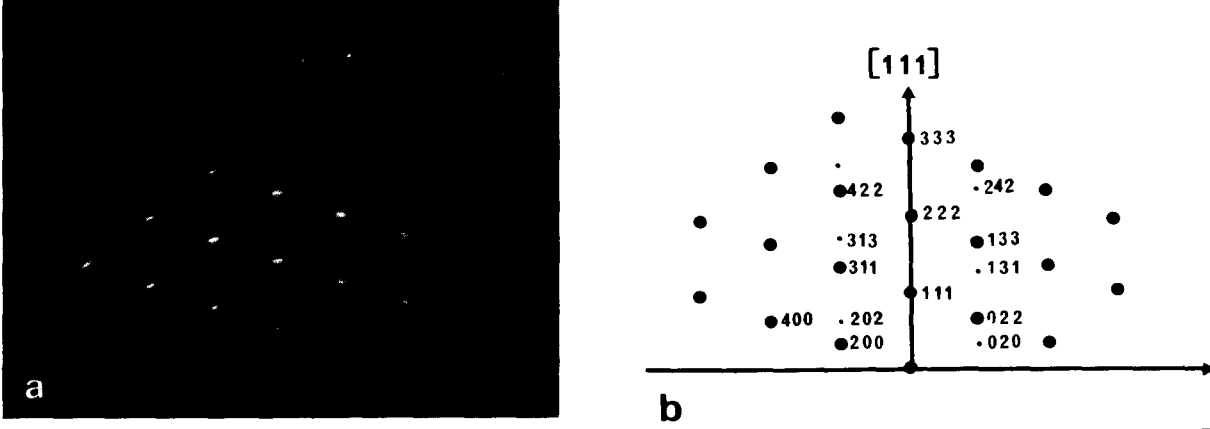


Fig. 8. Electron diffraction pattern of AlSb on CaF₂ (a) with indexation (b). Satellites near the main diffraction spots show the presence of twinning.



Fig. 9. Specular film of AlSb on GaAs (sample No. 211).

deposited which appears clearly on SEM photographs.

Fig. 8 shows the low angle electron diffraction pattern of AlSb epitaxially grown on CaF₂. It appears that the main diffraction peaks correspond to an azimuth |110|; the weak peaks correspond to the symmetrical orientation |110| with respect to the |111| axis.

 BaF_2 . BaF_2 seems to be a better substrate than CaF_2 and it has a lattice mismatch, Δa_0 , of 1.1%. However BaF_2 is less stable than CaF_2 and reaction occurs with aluminium gaseous species and the surface of the substrate is decomposed.

 $Ca_3Mn_2Ge_3O_{12}$. The lattice parameter of $Ca_3Mn_2Ge_3O_{12}$ is more than twice the lattice parameter of AlSb ($\Delta a_0 = 0.4\%$). Unfortunately the substrate is decomposed by the gaseous species.

 Al_2O_3 . Al_2O_3 is known to be a good substrate for many semiconductors. Thin films can be grown on $(0001)Al_2O_3$, but these films are polycrystalline (slightly textured for low thickness $<1 \mu m$).

GaAs. Semi-insulating Cr doped (100)GaAs was used as substrate. In spite of the difference in lattice parameters mirror-like epitaxial AlSb films (fig. 9) were grown when a graduate $AlAs_{1-x}Sb_x$ intermediate film was deposited between the substrate and the film. The experimental procedure differs slightly from the above described procedure. The substrate is heated under a H_2 and AsH_3 mixed atmo-

sphere up to the deposition temperature. Then TMA is admitted in the reactor. The flow of AsH₃ is slowly set to zero whereas the flow of TMSb is increased from zero to the experimental value (table 3). This alloys to grow an intermediate film which accommodates the lattice mismatch between AlSb and GaAs.

Fig. 10 shows AlSb on GaAs (sample No. 214). X-ray analysis of Al and Sb show good homogeneity. Ga and As appear in X-ray analysis as well as in electronic microprobe, which results from interdiffusion in the deposit occurring at 1055 K. The deposit contains a slight amount of As.

To avoid partial decomposition of the substrate, an H₂ + AsH₃ atmosphere is used before the deposition of AlSb. However, a slight decomposition of the GaAs substrate often happens and GaAlAsSb hillocks appear. Fig. 11 shows AlSb on 100 GaAs with microinhomogeneities.

Quantitative analysis by electronic microprobe showed that these hillocks have approximately the composition Ga_{0.6}Al_{0.4}Sb_{0.9}As_{0.1}.

5. Discussion and conclusions

MO-CVD was found to be a reliable method to grow thin films of AlSb and to avoid all the problems of aluminium reactivity and inhomogeneity which occur on growth from the melt. However MO-CVD is possible for $T > 1000 \, \text{K}$ and for a high Sb/Al ratio ($\gtrsim 20$), otherwise a parasitic phase $\Lambda l_4 C_3$ appears. Analysis of the system Al-Sb-C--H gives a thermodynamic background of the experimental features connected with the deposition of AlSb, AlSb + Al₄C₃, and AlSb + Sb.

Epitaxial films were grown on [111]CaF₂ and [100]GaAs. However, the lattice match is not good enough for high crystalline quality films. An improvement is expected when a substrate like GaSb with $a_0 = 6.095$ Å will be used. Unfortunately this compound starts to decompose at 550°C. The use of triisobutyl aluminium as MO, whose radical is more stable than CH₃, for the transport of Al could allow to grow AlSb at a lower temperature than in the present work. For instance the growth temperature could be 900 K where it is thermodynamically possible. These experiments are in progress and will be reported elsewhere.

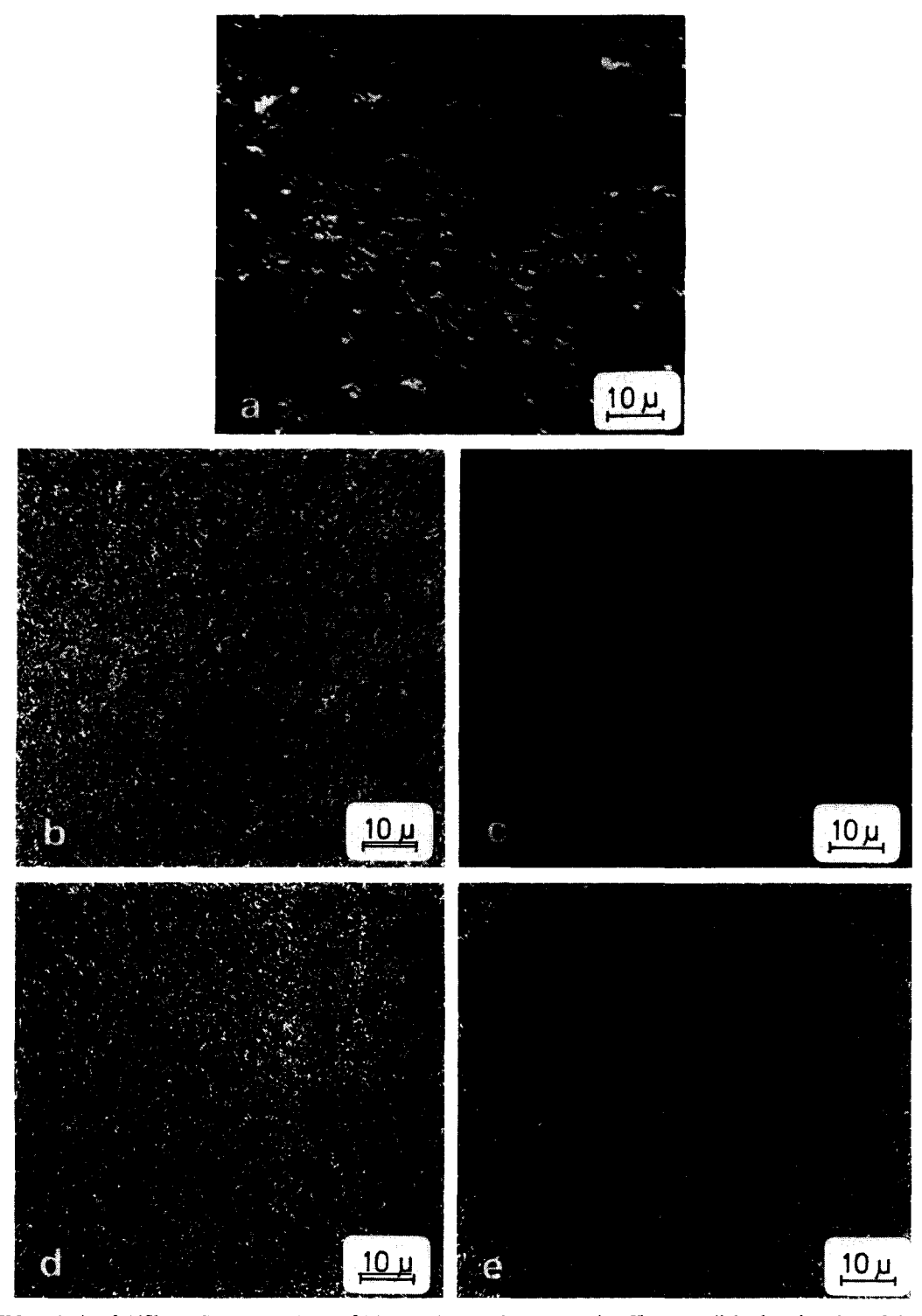


Fig. 10. SEM analysis of AlSb on GaAs (sample No. 214) showing good homogeneity. However slight deterioration of the surface due to instability of AlSb in air occurs. Due to lattice mismatch the deposit is under high degree of strain. Heating in the flux of electrons may sometimes result in separating the film from the substrate (a) surface morphology; (b)–(d) X-ray dispersive analysis $(Al(K_{\alpha}), Sb(L_{\alpha}), Ga(K_{\alpha}))$ and $As(L_{\alpha})$ respectively).

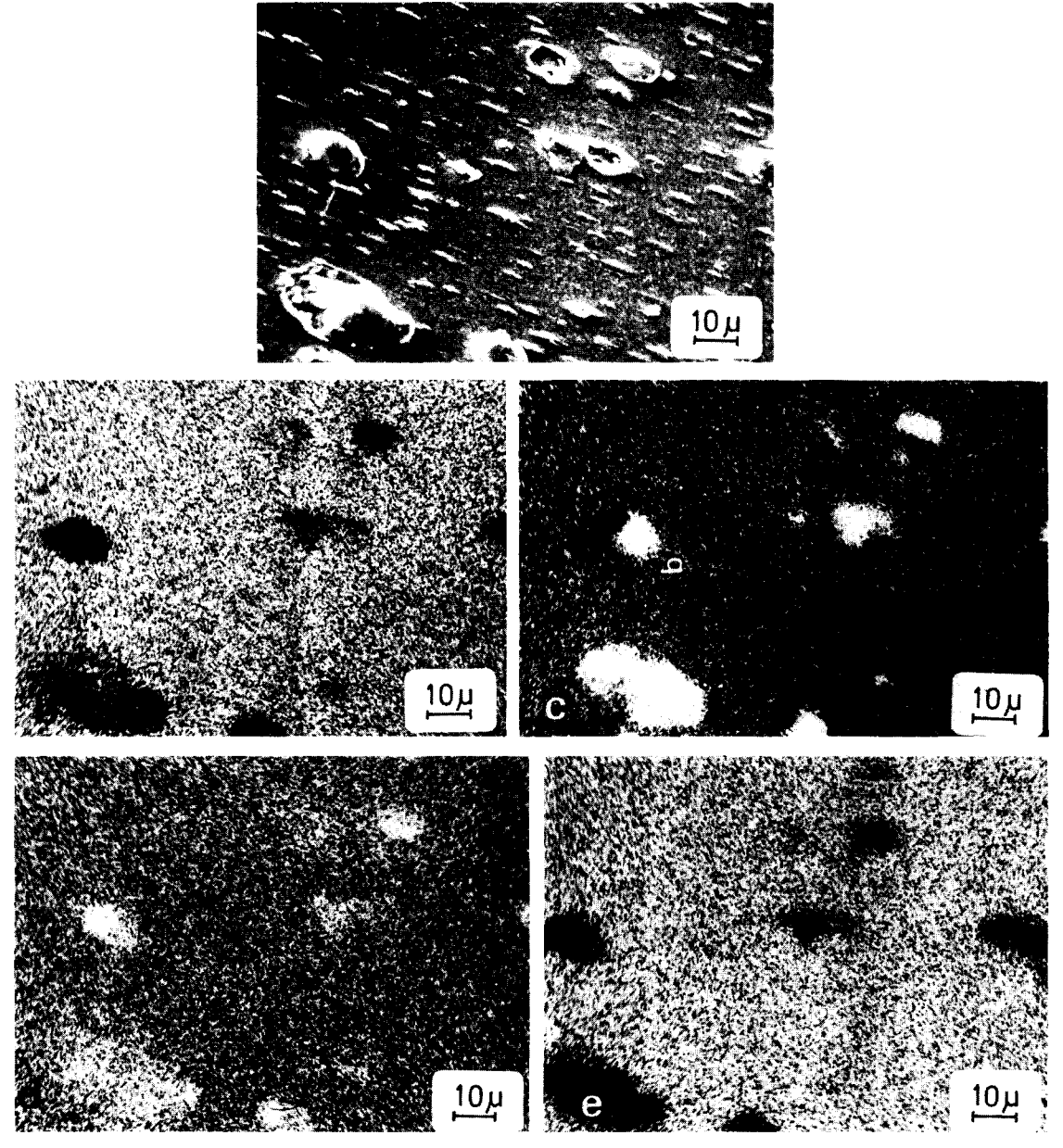


Fig. 11. SEM analysis of AlSb on GaAs (sample No. 216) showing $Ga_{1-x}Al_xAs_{1-y}Sb_y$ micronodules on the surface: (a) surface morphology; (b)–(e) X-ray dispersive analysis (Al(K_{α}), Sb(L_{α}), Ga(K_{α}) and As(L_{α}) respectively).

Acknowledgements

The authors wish to express their thanks to G. Nataf for kind helpful advices, to A. Malmanche and J. Rioux for the X-ray characterization, to R. Druilhe and L. Tertian for electron diffraction experiments,

M. Miloche for the SEM data, and to C. Crattepain for SIMS analysis.

This work was partially supported by the DGRST under contracts Nos. 76-7-1500 and 77-7-2025, and the SDTM (CNRS).

References

- [1] Review papers:
 - H.M. Manasevit, J. Crystal Growth 13/14 (1972) 306; 22 (1974) 125;
 - C.C. Wang, in: Proc. 6th Intern. Conf. on CVD, Proc. Vol. 77 (The Electrochem. Soc., 1977) p. 249.
- [2] See for instance, A.E. Middleton et al., US Natl. Tech. Inform. Serv., AD Report No. 769242/9GA (1973), and references therein.
- [3] A.V. Sandulova and E.L. Dolgov, Izv. Akad. Nauk SSSR Neorg. Mater. 3 (1967) 2003.
- [4] E. Passaglia, Material Sciences in Space, ESA Sp. (1976) 114, 401.
- [5] V.A. Presnov and V.F. Synorov, Soviet Phys.-Tech. Phys. 2 (1958) 104.
- [6] M.V. Koi and G.P. Sorokin, Soviet Phys.-Tech. Phys. 3 (1959) 1528.
- [7] J.E. Johnson, J. Appl. Phys. 36 (1966) 3193.
- [8] J.P. David, L. Capella, L. Laude and S. Martinuzzi, Rev. Phys. Appl. 1 (1966) 172.
- [9] M.H. Francombe, A.J. Noreika, S.A. Zeitman and J.E. Johnson, Thin Solid Films 32 (1976) 259.
- [10] N.J. Shevcik, J. Tejeda, C.M. Penchina and M. Cardona, Solid State Commun. 11 (1972) 1619.
- [11] G.A. Armantrout and J.H. Yee, in: Proc. Photovoltaic Solar Energy Conf., Berlin, 1979, p. 960.
- [12] M. Leroux, A. Tromson-Carli, P. Gibart and C. Vérié,

- in: Proc. Photovoltaic Solar Energy Conf., Berlin, 1979, p. 968.
- [13] J.J. Loferski, J. Appl. Phys. 27 (1966) 777.
- [14] P. Rappaport, RCA Rev. 20 (1959) 373.
- [15] See, for instance, H.J. Hovel, in: Semiconductors and Semimetals, Vol. 11, Solar Cells (Academic Press, New York, 1973).
- [16] C. Vérié, M. Leroux, A. Tromson and P. Gibart, in: Proc. Intern. Photovoltaic Solar Energy Conf., Luxembourg, 1978, p. 1033.
- [17] P.Y. Yu and B. Welber, Solid State Commun. 25 (1978) 209.
- [18] M. Leroux, Thèse 3ème cycle, Paris VI (1979).
- [19] W.H. Petzke, V. Gottschalch and E. Butter, Kristall Tech. 9 (1974) 209, 355, 477, 763.
- [20] K. Ziegler, K. Nagel and W. Pfhol, Ann. Chem. 629 (1960) 219.
- [21] C. Bernard, Y. Deniel, A; Jacquot, P. Vay and M. Ducarroir, J. Less-Common Metals 40 (1975) 165.
- [22] I. Barin, O. Knacke and O. Kubaschewski, Thermochemical Properties of Inorganic Substances, Suppl. (Springer, Berlin, 1977).
- [23] JANAF, Magnetic tape (1976).
- [24] JANAF, Thermochemical Tables (NSB, Washington, DC, 1971).
- [25] R. Hultgren, R.L. Orr, D. Anderson and K.K. Kelley, Selected Values of Thermodynamic Properties of Metals and Alloys (Wiley, New York, 1974).